UAV-Based Detection and Precision Management of Cirsium arvense: An End-to-End Workflow from Deep Learning to Variable-Rate Spraying

L. Moldvai[1,2*], P. Á. Mesterházi[2], G. Teschner[1] and A. Nyéki[1]

[1]*Department of Biosystems Engineering and Precision Technology, Albert Kázmér Mosonmagyaróvár Faculty of Agricultural and Food Sciences, Széchenyi István University, Hungary*

[2]*AXIÁL Ltd., Hungary*

successwolf80@gmail.com

A paper from the Proceedings of the

17th International Conference on Precision Agriculture and 11th Brazilian Congress on Precision and Digital Agriculture

13-15 July 2026

Porto Alegre, Brazil

Abstract

Unmanned aerial vehicle (UAV)–based weed detection enables site-specific herbicide application and reduced chemical input in arable cropping systems. This study presents an end-to-end workflow for the detection of Cirsium arvense and the generation of sprayer-compatible management zones under real field conditions. High-resolution RGB imagery was acquired using a multirotor UAV at 12 m and 25 m above ground level and supplemented with ground-based images. A YOLO-based single-class object detection model was trained on 800 annotated image tiles, augmented to 13,280 images, containing 92,544 weed instances, achieving a mAP@0.5 of 78.97%, an mAP@0.5–0.95 of 56.38%, a precision of 80.2%, a recall of 74.5%, and an F1-score of 77.2%. Detected weeds were projected into geographic coordinates using a marker-based geometric transformation, allowing the definition of minimum object buffer sizes for reliable spatial targeting. Precision spraying was successfully implemented, requiring herbicide application on 32.43% of the field area, resulting in a 67.57% reduction compared to full-area spraying. Post-treatment observations highlighted the influence of late-season application and cold weather on control efficacy. The results demonstrate the operational feasibility of UAV-guided precision weed management and provide a basis for future multi-species detection and higher-altitude UAV monitoring.

Keywords

UAV images, weed remote sensing, weed detection, YOLO, Site-Specific Weed Management (SSWM)

Introduction

Weeds impose severe agronomic and economic impacts, motivating precision control. In major crops, weed competition can reduce yields by 20–50% (e.g. ~40% loss in maize, 37% in rice, 36% in cotton) and incurs global economic losses on the order of $100 billion. These large losses persist despite $25 billion/year in herbicide (Esposito et al., 2021). Conventional broadcast herbicide spraying is inefficient and environmentally costly. Site-specific management (e.g. spot-spraying only where weeds occur) is recognized as an efficient, eco-friendly alternative (Zhang et al., 2021). For example, (Smith et al., 2019) emphasize that UAV-based mapping can optimize herbicide application and reduce chemical use.

Weed detection and management are critical issues in modern agriculture, as undesirable plants compete aggressively with crops for essential resources such as water, nutrients, and sunlight, often resulting in significant yield losses (Sandoval-Pillajo et al., 2025). For staple crops like Teff, uncontrolled weed growth remains a primary challenge, causing yield reductions that can reach up to 38% (Kebede et al., 2025). Historically, weed control relied on labor-intensive manual methods or the indiscriminate application of broad-spectrum herbicides, practices that have proven inefficient, costly, and environmentally detrimental, contributing to issues such as herbicide resistance and ecological pollution. To address these challenges and mitigate the negative impact on the environment and human health, Precision Agriculture (PA) has emerged, leveraging advanced technologies to enable Site-Specific Weed Management (SSWM). The core of SSWM is the accurate, timely identification and localization of weeds with CNN or YOLO algorithms to facilitate targeted interventions and significantly reduce chemical usage (Gallo et al., 2023).

UAVs equipped with cameras provide an efficient and versatile platform for non-contact monitoring, capturing high-resolution imagery over large agricultural areas (Das et al., 2025). These high-resolution images are crucial for developing detailed weed maps required for SSWC (Verbesselt et al., 2025). The advancement of computer vision and deep learning (DL) has revolutionized weed detection, offering automated, efficient, and accurate methods by capitalizing on the ability of DL models to handle complex spatial patterns within large datasets. Convolutional Neural Networks (CNNs) are a dominant architectural choice in computer vision tasks within agriculture. These models have demonstrated reliable performance in detecting and classifying weeds in various crops, distinguishing between different species and growth stages.

Nikolova et al. (2025) developed a UAV RGB imaging and pixel-based deep learning approach for early weed detection in maize, demonstrating that a DeepLabV3 model with a ResNet-34 backbone achieved the highest performance (precision, recall, and F1-score of 0.986; Kappa = 0.957). Field application revealed substantially higher weed infestation under subsoiling (4.6% of the area) compared to plowing (0.97%), highlighting the influence of tillage practices on weed emergence.

Accurate crop-row detection plays a pivotal role in spatially constrained weed mapping, as reliable discrimination between crop and weed locations is essential for estimating weed pressure and defining sprayable zones (Moldvai et al., 2025). However, this task is inherently challenging due to visual similarities between crops and weeds, missing plants within rows, and varying phenological stages throughout the growing season. Under high weed densities or advanced crop development, individual plants may visually merge, leading to contiguous regions that hinder object-level separation and compromise clustering-based row detection approaches. Such conditions can result in misleading spatial interpretations, particularly when conventional algorithms assume well-separated plant instances. To address these challenges, robust image preprocessing and adaptive instance-handling strategies are required to correctly interpret complex canopy structures and maintain reliable row geometry, especially in scenarios where precision weed control remains agronomically justified.

The final success of SSWM hinges not just on accurate detection but also on the ability to convert these results into actionable, localized field operations. Accurate projection of detections into geographic coordinates, often requiring centimeter-level geolocation accuracy provided by RTK-GNSS receivers, is essential for guiding precision equipment. Georeferenced individual detection points—such as those identifying C. arvense—must be efficiently converted into polygon-based management zones or shapefiles compatible with the target sprayer systems and other agricultural implements. This holistic methodology, integrating sophisticated YOLO-based object detection, rigorous data preprocessing, and precise georeferencing, provides a robust, efficient, and environmentally sustainable pathway for modern precision weed control.

Materials and methods

Study area and experimental design

The experiment was conducted in an agricultural field located close to Beled in Győr-Moson-Sopron, Hungary (coordinates: 47.4830115, 17.1089701) in a 24.61 ha area. Cirsium arvense populations occurred naturally across the field and were allowed to develop to growth stages suitable for visual detection from unmanned aerial vehicle (UAV) imagery. Three treatment areas were established: 1) precision spraying, guided by the proposed detection and management-zone generation workflow; 2) conventional full-area spraying; and 3) untreated control around the management-zone, used to evaluate the effectiveness of the precision treatment.

UAV platform, sensors and image acquisition

Image acquisition was performed using a multirotor UAV (Model: DJI Mavic 3 Multispectral) equipped with an RGB camera (image sensor: 4/3 CMOS, effective pixels: 20 MP, field of view: 84°, equivalent focal length: 24 mm, aperture: f2.8-f11 variable, focus: 1 m to infinity, shutter type: mechanical). Flights were conducted at two altitudes, 12 m and 25 m above ground level (AGL), selected to evaluate scale-dependent detection performance. All flights were conducted under stable sunlight conditions to minimize illumination variability.

The UAV was equipped with an RTK-GNSS receiver, enabling centimeter-level geolocation accuracy. Metadata recorded with each image included timestamp, latitude, longitude, altitude, UAV roll–pitch–yaw (RPY) angles, camera intrinsic parameters, five camera distortion coefficients, and gimbal orientation.

Dataset development and annotation

To build a robust object detection dataset, UAV imagery acquired at 12 m AGL was used. Only one class was defined: Cirsium arvense. All images were manually annotated using bounding-box labels in a self-developed tool, producing a dataset of 800 images with a size of 512 × 512 pixels, augmented to 13,280 images containing 92,544 annotated C. arvense instances.

Object detection model and training procedure

A YOLOv11 object detection architecture was used for target recognition. Model training was conducted on an NVIDIA GPU (model: GeForce RTX 2080 Ti, 11264MiB) using the Ultralytics framework (Ultralytics 8.3.179 Python-3.13.5 torch-2.8.0+cu129). Hyperparameters (learning rate, batch size, augmentation parameters, and number of epochs) were optimized empirically to achieve maximum detection precision.

Data augmentation included random flips, scaling and cropping, color jitter, mosaic augmentation, and synthetic augmentation. Model performance was evaluated using Precision, Recall, F1-score and mean Average Precision (mAP50 and mAP50–95).

Ground control markers and camera coordinate projection

To achieve precise projection of detections into geographic coordinates, we deployed high-contrast red paper markers (10 × 10 cm or 10 × 20 cm) distributed across the field. These markers served as ground reference points easily detectable by color thresholding in HSV color space. A custom program was used to detect the red markers, and their image-space pixel coordinates were extracted.

A projective transformation algorithm was implemented to convert detection pixel coordinates into geospatial coordinates (latitude/longitude).

The shapefile dataset contained multiple georeferenced reconstructions of the same ground marker, acquired from different viewing angles using a drone-based imaging workflow. To characterize their spatial distribution, centroid coordinates were generated for each reconstructed object in QGIS, followed by the computation of the overall mean center. A distance matrix was then derived to quantify the deviation of each measurement from this mean center.

The resulting distance values were further processed in Excel to obtain descriptive statistics, including the average and maximum distance. The maximum distance was subsequently applied as a minimum object buffer radius to ensure that the detected objects would fall within the designated management zone with high probability, thereby mitigating uncertainty arising from geometric projection effects inherent in drone imagery.

Generation of management zones and shapefile production

For agricultural implement compatibility, including the target sprayer system, detection points were converted to polygon-based management zones. Each georeferenced C. arvense detection was assigned a buffer radius, representing the area requiring localized herbicide application. All buffered regions were merged into a preliminary polygon layer. The first spraying experiment was unsuccessful: the sprayer monitor accepted the management zones but did not apply them.

It was realized that the problem was caused by manufacturer-specific requirements. The sprayer terminal required all management zones to be connected to the field boundary by a single continuous branch structure, similar to a minimum spanning tree topology, ensuring compatibility with the controller’s internal zone parser.

Algorithm for connectivity and hole bridging

A custom algorithm was developed to meet these constraints. First, a graph-based minimum branch construction was generated and added to the objects. Next, hole-to-border bridging was generated using narrow “bridges” that connected holes to the outer field boundary. This ensured that all sub-polygons became simply connected (no internal islands). This produced a single-component, topologically valid management zone suitable for shapefile export. Shapefiles were exported in WGS84 projection.

Spraying procedure

Precision spraying was conducted using a field sprayer capable of reading the generated management zone shapefiles (Machine: Berthoud Raptor 42.40, 30 m working width, sectioned every 50 cm. Monitor: Trimble GFX-1260, RTK accuracy, using the mAXI-NET 2.0 correction signal – approx. ±2 cm. Applied product / dose: Nufozat, 5 L/ha. Active ingredient: Glyphosate). Automatic nozzle control was calibrated to minimize overlap and ensure accurate spatial activation. Three treatment areas were implemented: precision treatment using the YOLO-generated shapefile; full-area broadcast herbicide application; and untreated control.

Post-treatment monitoring using UAV imagery

One month after herbicide application, the field was re-surveyed using the same UAV imaging protocol at 12 m and 25 m AGL. The resulting imagery was analyzed to assess survival or regrowth of C. arvense in each treatment plot, compare density reduction between precision and full-area spraying, evaluate potential drift or off-target impacts, and validate the operational success of the management zones and shapefile compatibility.

This post-treatment evaluation provided quantitative evidence of the effectiveness of the precision spraying workflow.

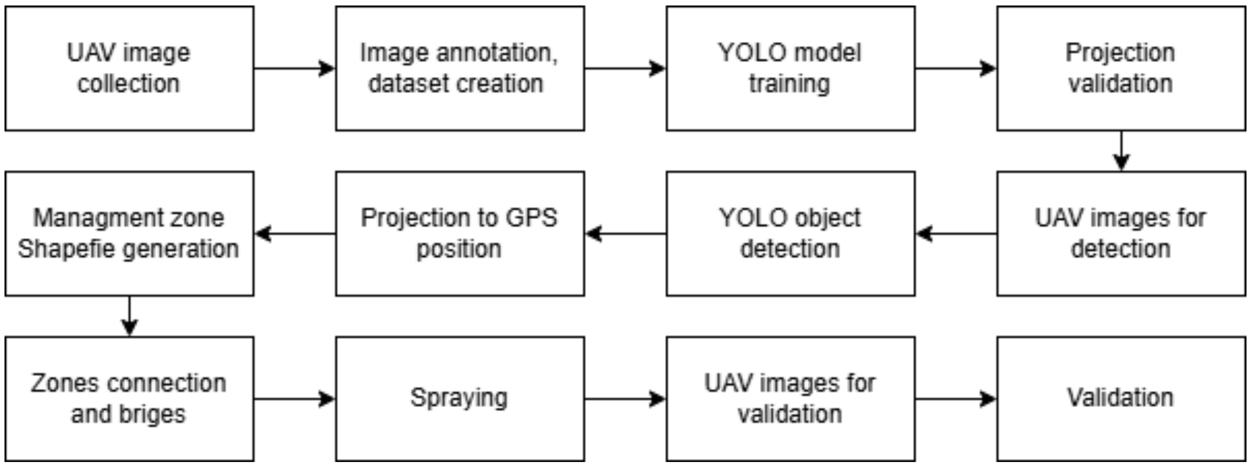

Figure 1. Experimental workflow

Results

Dataset establishment and image acquisition outcomes

At the beginning of the study, an experimental field was designated near Beled, Hungary, based on its history of severe Cirsium arvense infestation in previous years. This field was therefore considered well suited for evaluating a UAV-based weed detection and precision management workflow. However, the summer of 2025 was characterized by exceptionally dry weather conditions, which delayed weed emergence and resulted in substantially lower-than-expected infestation levels during the early part of the growing season.

Later in the season, more favorable rainfall conditions occurred, which led to a rapid increase in weed infestation at the original field site during autumn.

During the initial UAV campaign over the study area, imagery was acquired exclusively at an altitude of 12 m above ground level (AGL) to support both the construction and expansion of the image dataset. Following a preliminary analysis of these images, it was hypothesized that imagery captured from a higher flight altitude could still provide sufficient spatial detail for training a YOLO-based object detection model. Consequently, a second UAV flight was conducted at an altitude of 25 m AGL to evaluate the feasibility of scale-dependent detection performance.

For model development, a subset of the acquired images was subdivided into non-overlapping tiles of 512 × 512 pixels. All visible C. arvense individuals were manually annotated using bounding-box labels. In total, 800 image tiles were annotated, 13,280 augmented images were generated, resulting in 92,544 labeled bounding boxes representing individual weed instances.

Table 1: Measurement dates and aims.

Date	12 m	25 m	Aims
2025-09-04	310	0	Collect images for YOLO training.
2025-09-12	402	101	Collect images for YOLO training.
2025-09-30	403	266	For YOLO detection and shapefile generation
2025-10-27	400	0	Post-treatment assessment 1
2025-11-10	108	60	Post-treatment assessment 2

Object detection model performance and inference results

Using the constructed dataset, a YOLOv11n object detection model was trained to identify Cirsium arvense. The annotated dataset was randomly partitioned into three subsets: 70% for training, 15% for validation, and 15% for independent testing. This split ensured robust model evaluation while minimizing the risk of overfitting.

Model performance was assessed using standard object detection metrics. On the test dataset, the trained model achieved a mean Average Precision of 78.97% at an Intersection over Union threshold of 0.5 (mAP@0.5) and 56.38% when averaged across IoU thresholds ranging from 0.5 to 0.95 (mAP@0.5:0.95). The corresponding precision, recall, and F1-score values were 80.2%, 74.5%, and 77.2%, respectively. These results indicate a high level of detection accuracy, with a moderate trade-off between false positives and missed detections, which is typical for single-class weed detection under heterogeneous field conditions.

The trained model was subsequently applied to UAV imagery acquired on 30 September 2025 at a flight altitude of 12 m above ground level. To ensure compatibility with the network input size, the images were subdivided into 512 × 512 pixel tiles, and object detection was performed on each tile independently. The resulting bounding boxes and associated confidence scores were exported to a spreadsheet format for further processing and analysis.

Figure 2. The detected weeds.

Following detection, the pixel coordinates of all predicted bounding boxes were transformed back into the coordinate system of the original full-resolution images. These reconstructed image-space coordinates were then stored and used as the basis for subsequent geometric projection into georeferenced space and management-zone generation.

Projection accuracy and minimum object buffer determination

To enable spatially accurate management-zone generation, the detected object pixel coordinates had to be converted into geographic (GPS) coordinates. This back-projection process required accounting for multiple factors, including UAV flight altitude, camera orientation angles (roll, pitch, and yaw), camera intrinsic parameters, and lens distortion effects. To quantify the positional uncertainty introduced by these factors, a dedicated marker-based evaluation was conducted.

A series of reference image sequences was acquired over four high-contrast ground markers placed within the field. In total, 108 images at 12 m AGL were collected from varying viewing angles and image-plane positions, ensuring a representative range of geometric configurations, and 60 images at 25 m AGL. For each image, the marker pixel coordinates were extracted and projected into geographic coordinates using the same transformation pipeline applied to the weed detections.

The resulting georeferenced marker positions were exported as shapefiles and compared against their known true locations. The Euclidean distances between the projected positions and the corresponding ground-truth coordinates were calculated to quantify projection error. This positional deviation directly defines the minimum buffer radius required for each detected object to ensure that the true weed location is contained within the generated management zone with high confidence.

The projection accuracy analysis was performed separately for imagery acquired at 12 m and 25 m above ground level. The resulting distance statistics, including mean and maximum deviations, are summarized in Table 2 and Table 3, respectively. These results provided the empirical basis for determining the minimum object buffer size used in subsequent management-zone generation.

Table 2. Markers - 12 m above ground level

	Marker1	Marker2	Marker3	Marker4
Detection number	14	12	10	9
Average distance	0,163	0,628	0,399	0,616
Max distance	0,474	1,08	0,625	1,134

Table 3. Markers - 25 m above ground level

	Marker1	Marker2	Marker3	Marker4
Detection number	24	22	28	21
Average distance	1,007	1,102	1,159	0,819
Max distance	2,668	2,691	2,563	1,658

Management zone generation and shapefile topology correction

The list of detected objects was converted into geographic coordinates using the previously described projection procedure. Based on these georeferenced detection points, the empirically determined minimum object buffer was applied to each individual Cirsium arvense instance, resulting in an initial polygon layer representing the spatial extent of all detected weeds. This layer was exported as a shapefile containing all buffered weed objects.

Subsequently, a geometric union operation was performed on the buffered polygons, producing a preliminary management-zone shapefile that consolidated overlapping and adjacent weed buffers into continuous regions (Figure 3a). To account for the operational characteristics and spatial resolution of the spraying system, an additional buffer was applied to the unified polygons, ensuring sufficient coverage and minimizing the risk of untreated areas caused by nozzle spacing or control delays (Figure 3b).

In the next step, a single-line field boundary representation was generated, and all spatially isolated management-zone components were connected to this boundary using a narrow connecting structure derived from a graph-based minimum spanning tree algorithm. This procedure ensured that all polygons formed a single connected component, as required by the sprayer controller. Furthermore, internal holes within the polygon structure were connected to the outer boundary using narrow “bridge” elements, thereby eliminating internal islands and producing a topologically valid, simply connected management zone.

The final, controller-compatible shapefile, incorporating all connectivity corrections and hole-bridging operations, is shown in Figure 3c.

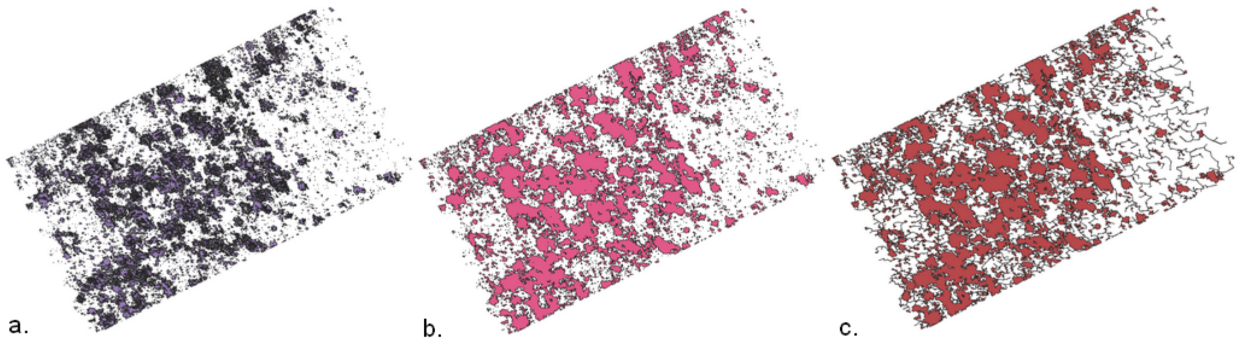

Figure 3. a) detected infested area; b) buffered management zones; c) connected zone aligned with the field boundary.

Spraying coverage and chemical savings

The potential reduction in herbicide use achievable through precision spraying is strongly dependent on the spatial extent and severity of weed infestation. In the present study, the experimental field covered a total area of 24.61 ha and exhibited a relatively high level of Cirsium arvense infestation. Based on the prescription map, the field was divided into precision-treated (7.40 ha), fully treated (14.83 ha), and untreated areas (2.38 ha).

Within the precision-treated zone, herbicide application was required on only 2.40 ha. This corresponds to 32.43% of the precision-treated area being sprayed, representing a chemical saving of 67.57% compared to conventional full-area broadcast spraying within the precision-treatment zone.

Figure 4 illustrates the spatial correspondence between the planned management zones and the actual sprayed area. The orange regions represent the areas where herbicide application was executed, as reconstructed from the operational data recorded by the sprayer controller. The green layer beneath shows the management zone converted into a field-boundary-based polygon representation. A strong spatial agreement between the planned and executed spraying areas is evident, demonstrating the successful implementation of the generated shapefile by the spraying system.

Importantly, the sprayer did not apply herbicide along the narrow connector paths, approximately 1 cm in width, that were introduced solely to satisfy controller-specific topological constraints. This confirms that these artificial connectivity structures did not result in unintended chemical application. Both spatial layers were overlaid on an orthophoto of the study area, providing a clear visual validation of spraying accuracy and system performance.

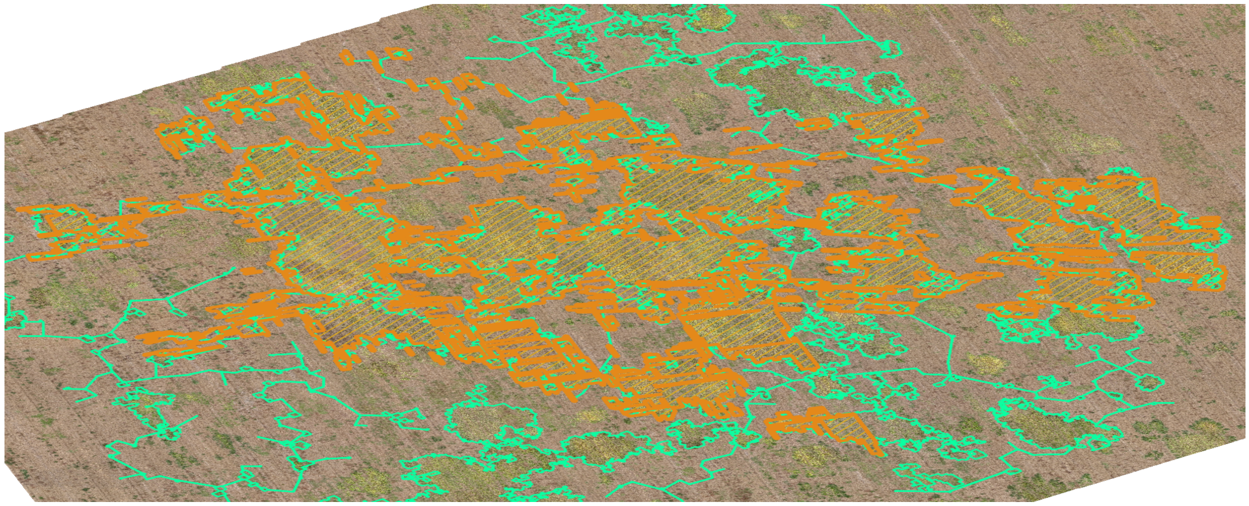

Figure 4. The spraying test with water. The green is the border of the management zone and the yellow are the places where spraying occurred.

Post-treatment field assessment and treatment effectiveness

Following herbicide application, the treated area was surveyed twice through on-site field inspections conducted by plant protection specialists, and two additional UAV-based surveys were performed. The timing of the treatment was suboptimal, as application occurred relatively late in the season and was followed shortly by the onset of colder weather conditions. These environmental factors influenced the observable treatment effects and complicated post-treatment evaluation.

For Cirsium arvense and Convolvulus arvensis, the treatment efficacy was limited. Cold-induced yellowing and partial plant senescence were observed not only in the untreated control areas but also within the fully treated plots, indicating that temperature stress contributed to visible plant damage independently of herbicide application. Furthermore, individuals of both species survived in certain locations even within the conventionally treated full-area plots, suggesting that the reduced treatment efficacy was not solely attributable to the precision spraying approach.

In contrast, the herbicide application was highly effective against other weed species present in the field, although these were not the primary target species of the study. No surviving individuals of these non-target weed species were detected within the sprayed areas, whereas they remained viable in the untreated zones.

Within the precision-treated areas, a spatially differentiated response was observed. Weed individuals located at greater distances from C. arvense patches frequently survived, while weeds in the immediate vicinity of detected C. arvense plants were effectively controlled. This pattern reflects the localized nature of the precision spraying strategy and the defined buffer-based management zones.

Although UAV imagery was acquired after treatment, the combined effects of seasonal senescence and cold stress limited the objective interpretation of these data. Consequently, post-treatment UAV-based assessments could not be reliably quantified, and treatment effectiveness was primarily evaluated through field observations.

Conclusion

This study demonstrated the feasibility of a UAV-based object detection and precision spraying workflow for the site-specific management of Cirsium arvense under realistic agricultural conditions. A YOLO-based single-class object detection model was successfully trained using a heterogeneous dataset comprising UAV and ground-based imagery. The trained model achieved an mAP@0.5 of 78.97%, an mAP@0.5–0.95 of 56.38%, and an F1-score of 77.2%, a precision of 80.2%, and a recall of 74.5%, indicating reliable detection performance despite variations in scale, viewpoint, and background complexity.

The integration of marker-based geometric projection enabled the conversion of image-space detections into georeferenced management zones with quantifiable positional uncertainty. This uncertainty analysis provided an empirical basis for defining minimum object buffer sizes, ensuring that detected weed locations were consistently captured within the generated spraying zones. A custom topology-correction algorithm was further developed to satisfy sprayer-specific shapefile requirements, allowing seamless operational deployment without unintended herbicide application along artificial connector paths.

From an agronomic perspective, the precision spraying approach resulted in herbicide application on approximately 32.43% of the precision-treated area, corresponding to a chemical saving of 67.57% compared to full-area broadcast spraying within the precision-treatment zone in a heavily infested field. This highlights the potential of UAV-guided weed management to substantially reduce input use even under unfavorable infestation conditions.

The post-treatment assessment also emphasized the influence of real-world environmental factors. Late-season application combined with the onset of cold weather limited herbicide efficacy for C. arvense and Convolvulus arvensis, demonstrating that detection accuracy alone cannot compensate for suboptimal agronomic timing. Such constraints are inherent to agricultural practice and underline the importance of integrating precision technologies with adaptive management strategies and appropriate application windows.

Future work will focus on extending the detection framework to imagery acquired at 25 m above ground level, enabling larger-area coverage and improved operational efficiency. Additionally, the development of multi-class, species-specific weed detection models represents a key research direction, with the potential to support selective, herbicide-type-specific treatments. Together, these advancements would further enhance the scalability, robustness, and agronomic relevance of UAV-based precision weed management systems.

Acknowledgments

The research was carried out by the "Precision Bioengineering Research Group", supported by the "Széchenyi István University Foundation". The research was conducted within the framework of the Cooperative Doctoral Program (KDP) Doctoral Student Scholarship. We would like to express our gratitude to the Ministry of Culture and Innovation and the National Research, Development and Innovation Office for their support.

References

Das, A., Yang, Y., & Subburaj, V. H. (2025). YOLOv7 for Weed Detection in Cotton Fields Using UAV Imagery. AgriEngineering, 7(10), 313. https://doi.org/10.3390/agriengineering7100313

Esposito, M., Crimaldi, M., Cirillo, V., Sarghini, F., & Maggio, A. (2021). Drone and sensor technology for sustainable weed management: A review. Chemical and Biological Technologies in Agriculture, 8(1), 18. https://doi.org/10.1186/s40538-021-00217-8

Gallo, I., Rehman, A. U., Dehkordi, R. H., Landro, N., La Grassa, R., & Boschetti, M. (2023). Deep Object Detection of Crop Weeds: Performance of YOLOv7 on a Real Case Dataset from UAV Images. Remote Sensing, 15(2), 539. https://doi.org/10.3390/rs15020539

Kebede, A. S., Muluneh, T. W., & Adege, A. B. (2025). Detection of weeds in teff crops using deep learning and UAV imagery for precision herbicide application. Scientific Reports, 15(1), 30708. https://doi.org/10.1038/s41598-025-15380-3

Moldvai, L., Mesterházi, P. Á., Teschner, G., & Nyéki, A. (2025). Aerial Image-Based Crop

Row Detection and Weed Pressure Mapping Method. Agronomy, 15(8), 1762. https://doi.org/10.3390/agronomy15081762

Nikolova, P. D., Evstatiev, B. I., Atanasov, A. Z., & Atanasov, A. I. (2025). Evaluation of Weed Infestations in Row Crops Using Aerial RGB Imaging and Deep Learning. Agriculture, 15(4), 418. https://doi.org/10.3390/agriculture15040418

Sandoval-Pillajo, L., García-Santillán, I., Pusdá-Chulde, M., & Giret, A. (2025). Weed detection based on deep learning from UAV imagery: A review. Smart Agricultural Technology, 12, 101147. https://doi.org/10.1016/j.atech.2025.101147

Smith, B. G., Faria Defeo, L., & Jensen, T. A. (2019). SITE SPECIFIC WEED MANAGEMENT MAPPING SYSTEM USING UNMANNED AERIAL VEHICLE (UAV). 2019 Boston, Massachusetts July 7- July 10, 2019. 2019 Boston, Massachusetts July 7- July 10, 2019. https://doi.org/10.13031/aim.201900207

Verbesselt, S., Daems, R., Willekens, A., & Van Beek, J. (2025). UAV Based Weed Pressure Detection Through Relative Labelling. Remote Sensing, 17(20), 3434. https://doi.org/10.3390/rs17203434

Zhang, J., Maleski, J., Jespersen, D., Waltz, F. C., Rains, G., & Schwartz, B. (2021). Unmanned Aerial System-Based Weed Mapping in Sod Production Using a Convolutional Neural Network. Frontiers in Plant Science, 12, 702626. https://doi.org/10.3389/fpls.2021.702626